Jiao, R., Yuan, X., Braun, J., Wang, Z. (2021): Thermo-kinematic modeling of the Cenozoic uplift of the Bogda Shan, Northwest China. - Tectonophysics, 816, 229031.

https://doi.org/10.1016/j.tecto.2021.229031

Thermo-kinematic modeling of the Cenozoic uplift of the Bogda Shan, Northwest China

Ruohong Jiao[a,*], Xiaoping Yuan[b,c], Jean Braun[c], Zongxiu Wang[d]

[a] *School of Earth and Ocean Sciences, University of Victoria, Canada*
[b] *Hubei Key Laboratory of Critical Zone Evolution, School of Earth Sciences, China University of Geosciences, Wuhan, China*
[c] *Helmholtz Centre Potsdam, GFZ German Research Centre for Geosciences, Potsdam, Germany*
[d] *Institute of Geomechanics, Chinese Academy of Geological Sciences, Beijing, China*

Abstract

Constraining the Cenozoic uplift of Tian Shan is important for assessing the impact of the India-Asia collision to Central Asia. Here we estimate the uplift history of the Bogda Shan, northeastern Tian Shan, using a thermo-kinematic model which is constrained by previously reported apatite fission-track thermochronological data. By assuming that the growth of the mountain range propagates towards the basin as a classic critical wedge model, we show that the observed variation in the cooling ages on the mountain flank can be used to provide constraints on the timing and rate of the deformation along a series of south dipping thrust faults, which all root on a low-angle décollement. Inverse modeling confirms previous findings from thermal history models that the late Cenozoic uplift in the Bogda Shan initiated during the Paleogene, no later than ∼40 Ma. Since the early Miocene (∼23 Ma), locus of uplift has expanded to the current southern margin of the Junggar Basin. Our kinematic model of the deformation of the Bogda Shan suggests a temporal stability in the shortening rate of the northeastern Tian Shan over the period of the India-Asia collision during the late Cenozoic.

Keywords: Mountain building, Thermochronology, Thermo-kinematic modeling, Fission-track, Tian Shan

1. Introduction

The collision between India and Asia started more than 50 million years ago (Rowley, 1996; Najman et al., 2010; Ding et al., 2016; Hu et al., 2016), and the far-field effect of the collision has caused significant deformation on the lithosphere of the Central Asia (e.g., Molnar and Tapponnier, 1975; Windley

*Corresponding author
Email address: rjiao@uvic.ca (Ruohong Jiao)

et al., 1990; Avouac et al., 1993; Morin et al., 2018). Understanding when and how the deformation took place requires constraining the Cenozoic uplift history of Tian Shan, the largest mountain chain in Central Asia. Many studies have documented a marked increase in the uplift or exhumation rates at $\sim$25 Ma or later on the Junggar margin of Tian Shan, much later than the onset of the India–Asia collision. However, it remains unclear if the apparent time lag between the initial collision and the recorded intracontinental mountain building reflects a northward propagation of the deformation (Tapponnier et al., 2001; Wang et al., 2008a), a later change in the configuration of the collision zone (Van Hinsbergen et al., 2012; Pusok and Stegman, 2020; Huangfu et al., 2021), or the heterogeneity in the mechanical property of the Eurasian plate (England and Houseman, 1985; Bian et al., 2020).

Deformation in continental collision zones often leads to significant exhumation of crustal materials, which can be used to track the evolution of an orogenic belt. Low-temperature thermochronology, as an effective tool for estimating mountain exhumation process, has been extensively applied in the study of the Cenozoic evolution of Tian Shan. Previous studies have reported various ages for the acceleration in the exhumation rate of Tian Shan (Figure 1a), ranging from the Paleocene to the late Miocene (e.g., Bullen et al., 2001; Hendrix et al., 1994; Sobel et al., 2006; Macaulay et al., 2014; Jolivet et al., 2010; Yu et al., 2014; Glorie et al., 2011). The variability in the thermochronological cooling ages has been suggested to reflect changes in the crustal shortening rate, which may be linked to different horizontal forces transmitted from the different stages of the growth of the Tibetan Plateau or the India-Eurasia collision (e.g., Glorie et al., 2011). In some parts of Tian Shan, studies have documented a migration of the deformation during the growth of the mountain topography, which were responsible for the variability in the ages recording the rapid exhumation events. For example in the southwestern Tian Shan, the Cenozoic exhumation started at $\sim$24 Ma in the mountain range (Figure 1a), and then the locus of exhumation propagated southwards towards the boundary of the Tarim Basin during the early Miocene (Sobel et al., 2006). However, it remains unclear whether the migration of the deformation occurred in association with the change in the crustal shortening across the mountain range, which have dominated in the crustal deformation of Tian Shan (Avouac et al., 1993; Yin et al., 1998; Yang et al., 2008).

Coupled modeling of the thermal and kinematic evolution of a mountain range provides a tool to quantify the lateral motion of crustal materials in a convergent tectonic setting (e.g., Herman et al., 2009, 2010; Batt et al., 2001; Coutand et al., 2014; Rak et al., 2017). Such applications require a good density of thermochronological ages distributed across the major structures that strike nearly perpendicular to the shortening direction. In the Tian Shan, one of such locations is the Bogda Shan, a narrow range in the eastern Tian Shan between the Junggar and Turpan Basins (Figure 1b). In the west, the Bogda Shan has a relatively simple structural setting, where the northern flank of the range represents as a curved fold-and-thrust belt (Figure 2a). Along this belt, the main south-dipping faults run generally parallel to the mountain range, and have been thrusting northwards towards the Junggar Basin (Figure 2b). These faults form a typical imbricate structure, likely merging onto the same décollement at depth (Li et al., 2016).

In this paper we use the western Bogda Shan as a laboratory to investigate how the crustal shortening may have controlled the uplift and exhumation pattern of an intracontinental orogen. We specifically test whether a significant change in the shortening rate is required to explain the large variability in the ages of exhumation acceleration reported from the region. We use a 2D kinematic model that is consistent with the basic orogenic mechanics to explain the uplift history of the mountain range, in which the current wedge-shapded mountain range was developed by the sequential growth of thrust faults. Based on the inverse analysis of a large number of simulations that minimize the misfits between the observed and model predicted apatite fission-track data, we provide constraints on the timing and rates of the Cenozoic deformation of the range.

2. Geological background

The oldest rocks of the Bogda Shan formed during the Carboniferous in a rift basin position between the Junggar and the Tarim blocks (Shu et al., 2011; Xie et al., 2016). The rifting was followed by a period of convergence during the middle Permian, when a succession of marine sedimentary rocks was accumulated in the western Bogda in an island-arc setting (Wang et al., 2018a). The paleo-oceanic trough was closed by the end of the middle Permian, followed by a period of collision during which the Permian and Mesozoic rocks were amalgamated (Tang et al., 2015; Ji et al., 2018; Wang et al., 2018a). Based on a regional-scale unconformity between the Middle and Late Permian strata and the abrupt change in the sedimentation environment between the two epochs, Wang et al. (2018a) suggested that Bogda Shan was initially uplifted by the end of the Middle Permian. However, petrological analysis of the Mesozoic strata in the Turpan Basin showed that the Lower Triassic deposits were derived from the continental crustal terrain south of the Turpan basin rather than the oceanic rocks in the Bogda Shan, suggesting that no significant topography existed between the Junggar and the Turpan Basins before the Early Triassic (Greene et al., 2005). Based on the zircon U-Pb spectrum in the Junggar deposition, Ji et al. (2018) suggested that the eastern Bogda Shan started to shed sediments into the basin during the Early Jurassic. In the western Bogda, paleocurrent observations on the Junggar and Turpan Basin margins indicate that the flow directions started to diverge from the present-day mountain top during the Late Jurassic, suggesting that part of the mountain had already been uplifted (Hendrix, 1992; Zhang et al., 2005). During the Cretaceous, no strong deformation occurred in regions throughout the eastern Tian Shan, and the area possibly experienced slow subsidence (Jolivet et al., 2018). On the southeastern margin of the Junggar Basin, the Cretaceous strata consist of sediments deposited in settings oscillating between fluvial, deltaic, and lacustrine environments (Gu et al., 2003), suggesting a generally low-relief topography in the western paleo-Bogda Shan.

Cenozoic uplift of the northern Tian Shan started no later than the late Oligocene, marked by contemporaneous increases in the sedimentation rate on the southern margin of the Junggar Basin at ∼26–22.5 Ma based on the magnetostratigraphy of a section on the piedmont (Ji et al., 2008) and rock cooling rate estimated using apatite fission-track thermochronology on the northern flank of the mountain at ∼25–24 Ma (Hendrix et al., 1994; Dumitru et al., 2001). Magnetostratigraphy of sediments in the Junggar Basin suggested a further increase of sedimentation rates during the Miocene (Ji et al., 2008; Charreau et al., 2009). West of Urumqi, the piedmont of northern Tian Shan features a ∼50 km-wide deformation zone consisting of three fold-and-thrust belts, which are currently absorbing a large portion of the deformation in Tian Shan (Yang et al., 2008). The deformation zone has accommodated about 6–12% of the total Cenozoic crustal shortening at this longitude across the entire width of the mountain range (Lu et al., 2019, and references therein), with the rest accommodated by structures further south in the interior of Tian Shan and on the northern margin of the Tarim Basin (Avouac et al., 1993). In the Bogda Shan of northeastern Tian Shan, previous thermochronological studies reported rapid Cenozoic exhumation events prior to ∼40 Ma (Wang et al., 2007, 2008b), at ∼30–20 Ma (Shen et al., 2008; Wang et al., 2008b), and after 19 Ma (Zhu et al., 2006; Wang et al., 2007, 2008b), but it remains poorly understood how these pulses of exhumation were related to the deformation pattern of the upper crust. In comparison to the region west of Urumqi, the northern piedmont of western Bogda Shan is relatively narrow (∼10 km), and the shortening rate across the foreland fold-and-thrust belt is much less significant (<1 mm/yr vs. 3–5mm/yr; Wu et al., 2016).

3. Apatite fission-track data in the western Bogda Shan

Fission-track analysis is a radiometric dating technique based on the observation of linear damages (i.e., fission tracks) caused by the fission decay of ^{238}U in the crystal grains. The density of chemically etched fission tracks is measured for determining an apparent cooling age, which can be complemented with the track length distribution to estimate the thermal path of a rock (see reviews by Tagami and O'Sullivan, 2005; Gallagher et al., 1998). Apatite fission-track (AFT) analysis can reveal the thermal history of a rock within the temperature range between ∼125–60°(Gleadow and Duddy, 1981), and is particularly useful for constraining the rock exhumation history during the mountain building process. In the Bogda Shan, previous studies reported AFT ages in a wide range between >150 Ma and <20 Ma (Tang et al., 2015; Gillespie et al., 2017; Wang et al., 2007, 2008b; Zhu et al., 2006), which contain information related to the Mesozoic and Cenozoic orogenic processes of the range.

In the western Bogda Shan, the reported AFT ages show a general northward younging trend towards the Junggar Basin boundary (Figure 2) (Tang et al., 2015). In the southwestern corner, the AFT ages in the Carboniferous and Permian terranes yield between 132 and 86 Ma, with all but one age older than 102 Ma (Figure 2a) (Tang et al., 2015). This age distribution is similar to the AFT ages collected to the immediate west of Urumqi (Guo et al., 2006), and both groups reflect the cooling phase of the terrane rocks during the late Jurassic–early Cretaceous. Across the northern flank of the western Bogda, the AFT age pattern is segmented by the main range-parallel thrust faults, i.e., the Erdaogou and Yamalike Faults (Figure 2a), across which the ages increase abruptly from the hanging wall to the footwall blocks (Figure 2b). On the hanging wall south of the two faults, the AFT ages yield younger than 40 Ma, indicating significant exhumation during the Cenozoic, which caused a partial or full removal of the Mesozoic partial annealing zone of the AFT system. The AFT ages on the footwall positions yield between 91 and 55 Ma, indicating much less exhumation during the Cenozoic. Samples near the Fukang Fault yield AFT ages in the Miocene, as young as 11.5 Ma.

The generally northward younging trend of the Miocene cooling ages suggests a propagation of the deformation center towards the Junggar Basin margin. If the Cenozoic deformation of the Bogda Shan has been predominantly accommodated by brittle motion on active structures, the marked variation in ages across faults most likely reflects a sequential (re)activation of the major structures from the core of the range to the basin boundary. This basin-ward growth pattern of the mountain range has also been observed in other parts of Tian Shan, such as the northern (Wang et al., 2009), the southwestern (Sobel et al., 2006), and the southern Chinese Tian Shan (Yu et al., 2014). In the Bogda Shan, this pattern is consistent with the observation that most of the Quaternary deformation and the recorded large earthquakes occur in the fold and thrust belt on the margin of the Junggar Basin (Wu et al., 2016).

Across the northern flank of the western Bogda Shan, the reported AFT ages (Zhu et al., 2006; Wang et al., 2007, 2008b), offer an opportunity to estimate the long-term fault slip histories and their roles in uplifting the mountain range. It is worth noting that in these analyses, the apatite grains were etched using 6.6–7% NHO_3 at 25 °C for 30–35 s, which is 10–15 s shorter than the standard protocol. The shorter etching duration could potentially lead to a $<10\%$ reduction of the track length (i.e., 1–1.5 μm length reduction for a 16 μm-long track; Seward et al., 2000). However, as the reported AFT ages in all three studies were calibrated using the Zeta method (Hurford and Green, 1983) against the age standards, we consider that the shorter etching time unlikely have observable impact on the AFT ages, which are determined based on track densities. The non-standard protocol could have a more considerable effect on the track length distribution. Therefore, in this study in order to avoid the potential bias on the modeling results introduced by the track length distribution, we only use the AFT age data to constrain the inversion of the thermo-kinematic models (Section 4.3).

4. Thermo-kinematic modeling of the Bogda Shan

4.1. The kinematic model

We build a 2D kinematic model to simulate the Cenozoic evolution of the Bogda Shan, which specifies the processes of both rock uplift, i.e., displacement of rocks relative to geoid, and surface uplift, i.e., the elevation increase of mountain range relative to geoid (as defined by England and Molnar, 1990). In a given period if the magnitudes of rock uplift and surface uplift of a mountain range can be estimated, one can also predict the amount of exhumation as the difference between the rock uplift and surface uplift (England and Molnar, 1990). We explain below how the rock uplift and surface uplift are implemented in our kinematic model.

We consider the crustal material in the mountain ranges as rigid blocks and thus the rock uplift is resulted completely from up throwing of the hanging wall rocks along the range-parallel thrust faults, which is proportional to the average slip rates on the faults for a given dip angle. We further assume that on the northern flank of the western Bogda Shan, the displacements on major faults, which are inherited from the Paleozoic and early Mesozoic orogeny (Allen and Vincent, 1997) and have accommodated all the crustal deformation across the range. These include several south-dipping thrust faults near the surface, i.e., the Erdaogou (F1), the Yamalike (F2), the Fukang (F3) faults from south to north (Figure 2), all of which root on a low-angle décollement (Sun and Wang, 2014; Wang et al., 2007). We ignore other smaller faults, as there are not enough ages across them and their perturbations of the AFT age pattern are less significant (Figure 2). Seismic reflection profiles show that the high-angle faults dip 45–65° towards the mountain, but the depth and the dip of the décollement are poorly constrained (Sun and Wang, 2014; Wang et al., 2007). In this paper we assume the high-angle faults are planar and dip at the same angle (γ; Figure 3), the value of which will be determined by inverse analysis. We also use inverse modeling to search for the optimal dip (β) of the décollement and the depth (D) where it intersects F1 (Figure 3a).

To simulate the slip history of the faults, we assume that the deformation of the mountain range propagates towards the basin in a piggyback style, represented as a sequential activation of thrust faults. Such deformation style can be readily inferred from the general basinward younging trend of the AFT ages (Figure 2b) and is consistent with the classic critical Coulomb wedge theory (Davis et al., 1983; Dahlen et al., 1984; Yuan et al., 2015), which assumes a wedge-shaped range when its surface slope reaches a critical angle. This mode is consistent with various sand analogue experiments where the material within the wedge deforms forward until a critical taper is attained, and continues to grow forward at a constant taper as additional material is encountered at the toe (e.g., Davis et al., 1983; Storti and McClay, 1995; Wu and McClay, 2011). This outward growth mechanism has been observed in many mountain ranges in convergent tectonic settings, including during the intracontinental deformation (e.g., Wang et al., 2014; Li et al., 2015).

Based on the imposed critical taper of the orogenic wedge, we also prescribe a surface uplift history of the mountain range in the kinematic model. During the period when a thrust fault is active, the up throwing of the hanging wall rocks drives the surface uplift, which is restricted to the hanging wall side of the fault (e.g., Figure 3b). During this period, the surface of the mountain flank is being tilted towards the basin, presenting a basinward decrease in the surface uplift rate of the hanging wall block. Increase of the elevation is assumed to be linear until the surface slope reaches the critical angle, after which the area of surface uplift will extend towards the basin associated with the (re)activation of the next fault closer to the basin. Note that on the hanging wall as the rock uplift velocity is spatially uniform (Figure 2b) or increase towards the active thrust fault (Figure 2c), increase of the surface slope means that the erosion rate on the hanging wall block increases towards the fault. This prediction is consistent with the AFT age pattern, which presents a younging trend within each fault block (Figure 2b).

From the imposed kinematic model, we can predict the exhumation history of the rocks along the mountain flank. The continuous shortening of the mountain range and the evolution of the topography towards the critical slope angle result in a history of exhumation, and the exhumation rate is calculated as the difference between the rock uplift and surface uplift. As the deformation propagates towards the basin and the frontal thrusts are activated consecutively, the velocity field of the rocks internal of the orogenic wedge evolves through time. Particularly, when the next thrust closer to the basin is activated, the location of the maximum uplift migrates to the hanging wall rocks near this thrust. Uplift of rocks behind the former, abandoned thrust fault still continues albeit possibly at a reduced rate (Figure 3). Therefore, the exhumation history of a rock may be controlled by displacements along more than one fault. This also demonstrates the necessity of using a 2D kinematic model, rather than a 1D exhumation model that could be directly inferred from the thermochronological cooling ages, to estimate the fault slip history in the orogenic wedge.

Here we provide a detailed description of the parameters that are used to define the kinematic model, and the optimum values of these parameters will be constrained by inverse analysis. We initiate the mountain range as a low-relief topography that has an initial surface slope of α_0 (Figure 3a). The Cenozoic uplift started at time T1, and the slip rates on both the décollement and the fault F1 are prescribed as V1 (Figure 3b). In the region near the axial surface between F1 and the décollement, the velocity field of the hanging wall is calculated as the average of the velocities along fault planes, ensuring an approximate mass conservation (Braun et al., 2012). The first stage of uplift continues from T1 to T2, when the slope of the mountain surface south of F1 reaches an assumed critical angle (α_c; Figure 3b). Then, starting from T2, the décollement propagates away from the mountain and the frontal fault F2 becomes active, while the slip rates on both the décollement and F2 change to V2. The height of the mountain range continues to grow, but the surface slope is restricted to $\leq \alpha_c$. Similarly, the second stage ceases at time T3, when the mountain surface south of F2 reaches the critical angle (Figure 3c). The last stage starts at T3 and continues until the present-day time (Figure 3d), during which the fault F3 is active and the slip rates on the décollement and F3 are V3. During the propagation of the deformation towards the basin, we impose that the slip rate on the décollement has either remained constant or increased, as the current understanding of the deformation history of Tian Shan does not support a decrease in the crustal shortening rate during the Cenozoic (e.g., Sobel et al., 2006).

4.2. The thermal model

In order to constrain the parameters in the kinematic model, we couple a thermal model of the crust to the kinematic model to predict the AFT cooling ages, which can be compared to the observations. The parameters in the thermo-kinematic model, e.g., the fault slip rate and model convergence rate, can be constrained by minimizing the misfit between the model prediction and observed data through a formal inversion process. In the model we built, the convergence rate is allowed to vary when the deformation propagates from one fault to another (see section 4.3).

We predict the thermal evolution of the crust by solving the heat-transfer equation using a finite-element method, Pecube (Braun, 2003; Braun et al., 2012). As the deformation of the mountain range continues, the geothermal isotherms are constantly perturbed by the motion of the rock particles, including both uplift and basin-ward advection, and the changing topography, and therefore the temperature field of the model is updated in every step. For rocks that eventually end up at the surface at 0 Ma, we track their positions and cooling paths in the kinematic model and the evolving temperature field, respectively. Then the AFT data are computed using the annealing model of Ketcham et al. (1999). Based on organic matter maturity in the strata, the late Cenozoic paleo-geothermal gradients in the Junggar Basin and the Bogda Shan foreland were estimated to be between 26 and 24°C/km (Wang et al., 2008b). Here we impose a geothermal gradient of ∼20–28°C/km at the beginning of the model, by prescribing the temperatures to 20°C at the sea level (0 km) and 400–550°C at the base of the model (−18 km).

4.3. Inverse analysis

To optimize the kinematic model, we conduct inverse analyses to constrain the values of the unknown parameters, namely the depth D and the dip β of the décollement, the dips γ of the high-angle thrusts, the initial (α_0) and critical (α_c) angles of the surface slope, the onset timings (T1, T2 and T3) and slip rates (V1, V2 and V3) of the three thrust faults in the model, the basal temperature of the model, and the AFT age unaffected by the Cenozoic uplift. The sampling ranges for these parameters are listed in Table 1. Inversion for the parameters is performed using the Neighborhood Algorithm (NA) (Sambridge, 1999b), a method for iteratively searching a multi-dimensional space to find acceptable models that can adequately reproduce the input observations. At each iteration, the forward model is run to predict the AFT ages, which are compared to the observations using the misfit function defined as

$$\phi = \sum_{i=1}^{n} (\frac{p_i - o_i}{\sigma_i})^2 \,, \tag{1}$$

where n is the number of AFT ages, p_i are the predictions, o_i are the observations, and σ_i are the uncertainties (∼8–20%) of the observations. To constrain the 2D kinematic model, the AFT ages on the northern flank of the mountain are projected on the model transect according to their location relative to the surface exposure of the major faults (Figure 2). For each inversion, the sampling comprises 800 iterations. The first iteration contains 1,000 simulations and every other contains 250; the resampling ratio is 0.8. After the sampling stage, the acquired ensemble is appraised using a Bayesian approach (Sambridge, 1999a) to estimate the marginal probability density functions (PDF) of the sampled parameters.

4.4. Results

The expected parameter values estimated from the sampled assemblages are summarized in Table 1 and presented as PDFs along the scatter plots (Figure 4). In general, the inversion shows good convergences for most of the parameters (Figure 4), but local minima are present for parameters used to define initial thermal structure of the model (Figure 4f).

For the slip history of F1 and F2, the inversion results suggest onset times prior to 40 Ma and between 26 and 34 Ma, respectively, whereas the slip rates for both faults are confined to <0.4 km/Ma (Figure 4a and 4b). For the last stage of uplift, the displacement on the current basin-boundary Fault (F3) is predicted to start between 19 and 26 Ma (T3). The slip rate (V3) on F3 is constrained between 0.3 and 0.7 km/Ma, which is consistent, within the uncertainty, with the earlier slip rates on the other faults (Figure 4c).

For the geometry of the structures, the inversion results suggest $>40°$ dip angle for the thrusts (Figure 4h), consistent with the observation from geophysical data (Sun and Wang, 2014; Wang et al., 2007). As one can expect, the modeling results show an apparent trade-off between the dip angle and the depth of the décollement, with the former constrained to $>9°$ and the latter (at the intersection with F1) at $\sim$7–13 km, respectively (Figure 4e). The inversion is not very sensitive to the values of the unreset pre-Cenozoic AFT age or the basal temperature of the crust model, which have been estimated at 82–132 Ma and 415–499°C, respectively (Figure 4f). The inversion results suggest a low angle ($<3°$) for the initial surface slope, and the critical slope angle is suggested at $\sim 5°$, similar to the present-day slope angle of the range.

The best-fit model from the inversion predicts AFT ages consistent with the age pattern observed along the mountain flank (Figure 5a), except that the scattered ages on the hanging wall of the Yamalike Fault (F2), i.e., at distance between 25 and 29 km on the transect (Figure 5a), cannot be reproduced. We suspect that this scattering of the observed AFT ages is due to the activities of the minor structures in this region (Figure 2a), which were not incorporated in the model setup but could have been displaced during the uplift of the mountain. For most samples, the predicted track length distributions are also similar to the observations (Figure 5b), despite that the length data were not used as constraints in inverse analysis. For some samples in the fossil partial annealing zone (e.g., W1 and W9; Figure 5b), the model predicts a bimodal distribution, but the peak of shorter track lengths is not shown in the observed distribution.

This difference may reflect the impact of the shorter etching time during the fission-track analysis.

Figure 6 shows the predicted exhumation histories of representative samples on the different structural blocks. The most significant exhumation occurs in the core of the range on the hanging wall of the Erdaogou Fault (F1; Figure 6a), where the Cenozoic exhumation has already removed more than 6 km thick crust and thus should have completely removed the AFT partial annealing zone prior to the Cenozoic orogeny. In this region, it is also worth noting that after 30 Ma even when the Erdaogou Fault (F1) became inactive, there was only a minor decrease in the exhumation rate. This is due to continuous shortening across the mountain range, which drives all rocks in the orogenic wedge towards the surface. In contrast on the footwall of the Erdaogou Fault, the rock exhumation magnitude has been much less significant as it did not start until the deformation propagated to the Yamalike Fault (Figure 6b–6c). On the hanging wall of the Fukang Fault (F3), the Cenozoic exhumation magnitude is predicted to increase towards the basin, due to the higher erosion rate of rocks near the mountain front (Figure 6d–6f).

5. Discussion

5.1. Cenozoic uplift, exhumation and shortening of the Bogda Shan

The northern flank of the Bogda Shan consists of terrane blocks separated by the high-angle thrust faults. Our thermo-kinematic modeling results confirm that the observed thermochronological data are compatible with the forward sequential growth thrusts (Figure 5a). On the footwalls within ∼3 km from the Erdaogou and the Yamalike Faults, the models predict <4 km total exhumation (e.g., sample X142-2; Figure 6b), suggesting that the magnitude of the late Cenozoic exhumation has not been enough to completely remove the fossil AFT partial annealing zone; this is consistent with the large variability presented by the AFT ages (all >30 Ma) in these areas (Figure 5a). Our results predict that the Cenozoic uplift of the Bogda Shan initiated prior to ∼40 Ma as thrusting on the Erdaogou Fault, leading to a period of rapid uplift in the currently highest part of the mountain (Figure 6a). This is in agreement with the conclusions from thermal history modeling of individual samples (Zhu et al., 2006; Wang et al., 2007), which estimated that the first stage of Cenozoic cooling of the mountain range occurred at 47–31 Ma. Our inverse modeling also demonstrates that the estimated timing for the onset of the Cenozoic exhumation cannot be further narrowed by the current data (Figure 4a). The late Eocene–early Oligocene onsets of exhumation have also been reported in other locations of Tian Shan (Figure 1a). Thermal history modeling of the AFT data from the Qiaoerma Granite in the central Tian Shan revealed a phase of exhumation starting in the Eocene at ∼50 Ma (Wang et al., 2009). Near this site, the AFT data also recorded a rapid cooling phase from ∼40 Ma (Domain G in Dumitru et al., 2001). In the southern Tian Shan, modeling of apatite (U-Th)/He data suggested rapid cooling around ∼40 Ma for rocks close to the Kuqa Depression

Boundary Thrust (Yu et al., 2014). Therefore, the Eocene–early Oligocene exhumation in Tian Shan are not localized events (e.g., Jolivet et al., 2010), suggesting that the far-field effect of the India-Eurasia collision started to cause deformation in Central Asia no later than the late Eocene. The initial stage of deformation perhaps only affected small regions which are currently in the interior of the mountains, and thus thermochronological records of this stage can only be retrieved from samples collected at relatively high elevations near peaks of some ranges, e.g., Bogda Shan, northern and southern Chinese Tian Shan (Figure 1a).

As the growth of orogenic wedge continued after the first stage of uplift south of the Erdaogou Fault and the locus of deformation migrated towards the basin, our modeling suggests that the Yamalike Fault was activated during the late Oligocene–earliest Miocene (Figure 4b). Uplift of the mountain extended to the current boundary of the Junggar Basin by $\sim$23 Ma, and since then has been mainly accommodated by the movement of the Fukang Fault. Based on thermal history modeling using data from single samples in western Bogda, an Oligocene-early Miocene acceleration in exhumation rate was not identified (Wang et al., 2007). However, in the eastern Bogda Shan, thermal history modeling of AFT data suggested rapid cooling between 30 and 20 Ma (Wang et al., 2008b). This late Oligocene–early Miocene exhumation event has also been reported extensively throughout Tian Shan (Figure 1a), such as in southwestern Chinese Tian Shan on the northwestern margin of the Tarim Basin (Sobel et al., 2006), in northern Tian Shan on the southern margin of the Junggar Basin, in the central Kyrgyz Tian Shan on the margin of the Issyk Kul intermontane basin (Macaulay et al., 2014), in the western Chinese Tian Shan on the margin of the Zhaosu Basin (Wang et al., 2018b), and in the Kyrgyz South Tian Shan suture zone (Glorie et al., 2011). Most of these records (except that in the Kyrgyz South suture zone) are located near the boundary between the main range and a foreland or intermontane basin. Assuming an outward growth model for most of the ranges in Tian Shan, the extensively reported late Oligocene-early Miocene exhumation along the current basin margins was likely subsequent to the initial deformation of the ranges in their core zones.

Rocks near the Fukang Fault (e.g., W7) yield the youngest AFT ages ($<$20 Ma) due to the more recent onset of the uplift and increased exhumation rate during the past 10 million years (Figure 6f). Note that when a rock transfers at a constant velocity through the axial zone between the shallow-dipping décollement and the steeper frontal thrust, its exhumation rate increases as the direction of motion of the rock particle changes upwards (Figures 3c and 3d). Given a proper combination of the fault slip rate and geometry, this acceleration in exhumation rate could be recorded by the cooling history of the rocks exhumed near the front of the wedge. For example, in our best-fit model, the initial exhumation of the sample W7 started at $\sim$23 Ma when the displacement on the Fukang Fault (F3) started, and then the sample experienced a further increase in exhumation rate at $\sim$14 Ma when it passed throughout the axial zone between the décollement and the frontal thrust. This second increase in exhumation rate postdates the onset of the deformation on the frontal thrust, and its magnitude is dependent on the difference in the dipping angles of the frontal thrust near the surface and the décollement at depth. This observation highlights the importance in incorporating kinematic models into the interpretation of rock cooling paths inferred from thermochronological data, and predicts that in some locations, a further increase in the exhumation rate may be observed after onset of the deformation, such as that observed in the Alai Range in the western Kyrgyz Tien Shan (Bande et al., 2017) and in the Baluntai section in the southeastern Tian Shan (Lü et al., 2013).

The modeled slip rates on the thrust faults have remained similar (~0.4–0.5 km/Ma) when the deformation propagated towards the Junggar Basin (Figure 4a–4c). Assuming that the crustal shortening across the Bogda Shan has been mainly accommodated by slipping on the low-angle décollement and major thrusts, to ensure mass conservation, the components of the displacements on the thrust and on the décollement perpendicular to the axial surface (an interface between the hanging wall and the material sliding on the décollement) should be equal to each other (Yuan et al., 2017). Based on such a relationship, we estimate a relatively stable shortening rate at ~0.45–0.6 km/Ma using the dip angles of 15°, 43°and 45°for the décollement, the thrust faults and the axial surfaces, respectively. Therefore, although reconstructions of the plate motion history indicate a change in the setting of the India-Asia collision zone around 25–20 Ma (Van Hinsbergen et al., 2012; Pusok and Stegman, 2020), our models suggest that such a change may not be recorded by the deformation of the Bogda Shan.

5.2. Sedimentary records in the Junggar Basin in response to the Cenozoic uplift

The Cenozoic exhumation history of the Bogda Shan and northern Tian Shan has been recorded by sedimentation history in the southern Junggar Basin. The initiation of Cenozoic uplift is reflected by a change in the paleoenvironment condition. On the southern margin of the Junggar Basin, occurrence of thick calcrete layers during the Paleogene indicate a semiarid climate and a lack of significant uplift or subsidence in the region (Heilbronn et al., 2015). The calcareous deposits disappeared by the late Eocene–early Oligocene, implying an increase in subsidence rate in the Junggar Basin (Jolivet et al., 2018), likely due to the initiation of the Cenozoic deformation of northern Tian Shan (Ji et al., 2008). During the Oligocene, an important change in the basin subsidence and sedimentation is marked by a regional unconformity, which were overlain by coarse clastic sediments and conglomerates (Windley et al., 1990; Allen et al., 1991). To the north and south of the Bogda Shan, the Oligocene unconformity and coarse-grain latest Oligocene or earliest Miocene sediments and conglomerates were also observed in the southern Junggar Basin (Liu et al., 2004) and Turpan Basin (Shao et al., 1999), respectively. Therefore, such a sedimentary record suggests that their main source region experienced a significant increase in uplift rate during the Oligocene–earliest Miocene.

Based on the velocity field of the rock particles in our kinematic model and the development of the shape of the orogenic wedge, we can calculate the sediment flux from the model transect (assuming a 2 km width of the transect) during the evolution of the mountain range (Figure 7). This calculation is useful to demonstrate, of the first order, how the mountain uplift and associated exhumation could influence the sedimentation rate in the foreland basin. Our calculation suggests that during the early Miocene, the sediment flux from the mountain range has increased significantly, when the shortening rate across mountain remains relatively stable. This change in the sedimentation history is due to the outward expansion of the mountain, which enlarged the area of erosion. This prediction is in agreement with sedimentary facies and magnetostratigraphy recorded by the Cenozoic stratigraphy in the southern Junggar Basin, which suggest an important change in the depositional environment and an increase in the sedimentation rate during the late Oligocene–earliest Miocene (Ji et al., 2008). Prior to the Oligocene, the uplift of Tian Shan might have been restricted to a narrow zone: to the west of Urumqi, this might be the area near Central Tian Shan (Figure 1b) (Dumitru et al., 2001; Jia et al., 2020), whereas in the western Bogda, this could be to the south of the Erdaogou Fault (Figure 2a). The uplift in such small regions would have resulted deposition much less considerable than that caused by the more extensive uplift along the southern margin of the Junggar Basin since the late Oligocene–earliest Miocene.

It is also worth noting that the sediment flux history predicted by our model does not replicate the pulses of sedimentation during the middle and late Miocene (Figure 7). This discrepancy suggests that other processes which are not considered in our kinematic model also contribute to the sedimentation in the southern Junggar Basin. It may be due to the different structural setting between the northern Tian Shan, where the sediment mainly derived from, and the western Bogda Shan. The northern Tian Shan is a mountain range much wider than the western Bogda and therefore the uplift could have been accommodated by more structures, including the (re)activation of the range-parallel thrust fault in the fold and thrust belt on the piedmont during the middle Miocene (Yu et al., Unpublished results). Another possible cause for the high sedimentation rate is climate change. The global cooling and drying since the late Miocene (Herbert et al., 2016), together with the rising topography of the mountain ranges in the region, have led to establish the modern arid climate in Central Asia with seasonal precipitation (Caves et al., 2017). This transformation in the regional climate was coincident with the acceleration in the sedimentation rate in the southern Junggar Basin, indicating that the increased seasonality and transience of the climate may be responsible for the high sedimentation rate since the late Miocene.

6. Conclusion

We elucidated the Cenozoic uplift history of the Bogda Shan using a simple thermo-kinematic model, which assumes that the mountain deformation has been accommodated by slipping on a low-angle décollement and multiple frontal thrusts. The model is constrained by AFT data across the northern flank of the range, and is optimized through a formal inverse analysis. Our results suggest that the Cenozoic uplift and exhumation of the western Bogda Shan started no later than ∼40 Ma. The locus of the deformation propagated northwards from the interior of the orogen towards the Junggar Basin, and arrived at the current basin boundary fault at ∼23 Ma. During this process, deformation of the mountain range could have been driven by crustal shortening at a relatively constant rate. The outward expansion of the mountain range could significantly increase the sediment volume eroded from the uplifted areas, which is consistent with the first increase in the sedimentation rate in the southern Junggar Basin during the latest Oligocene.

Acknowledgment

Apatite fission-track data used in this paper were published previously and available through Zhu et al. (2006), Wang et al. (2007) and Wang et al. (2008b). Jiao received support from the Natural Sciences and Engineering Research Council of Canada (Discovery Grant 2019-00243). Yuan's contribution was funded by the COLORS project from TOTAL. The GLIC Cluster in GFZ Potsdam was used for running simulations. We thank Kai Cao, Ed Sobel, Marc Jolivet, Pierre Valla, and anonymous reviewers for their criticism and suggestions on the manuscript.

Table 1: Model parameters sampled in inversion.

Parameter	Sampled range	Unit	Mean±std. error (best-fit)
Onset time of F1 (T1)	[30; 50]	Ma	45.9±3.3 (49.3)
Slip rate on F1 (V1)	[0; 1]	km/Ma	0.39±0.17 (0.36)
Onset time of F2 (T2)	[20; 40]	Ma	29.6±3.9 (29.4)
Slip rate on F2 (V2)	[0; 1]	km/Ma	0.48±0.20 (0.36)
Onset time of F3 (T3)	[0; 30]	Ma	22.5±3.5 (23.3)
Slip rate on F3 (V3)	[0; 1]	km/Ma	0.52±0.19 (0.38)
Dip angle of thrusts (γ)	[30; 60]	°	47.3±6.9 (43.0)
Décollement depth at F1 (D)	[−15; −5]	km	−9.9±2.9 (−11.5)
Décollement dip (β)	[0; 20]	°	13.2±3.8 (14.8)
Initial surface slope (α_0)	[0; 5]	°	2.4±1.3 (2.7)
Critical surface slope (α_c)	[5; 7]	°	5.4±0.5 (5.0)
Model basal temperature (Tp_b)	[400; 550]	°C	457±42 (476)
Unreset apatite FT age (Age_0)	[100; 150]	Ma	107±25 (117)

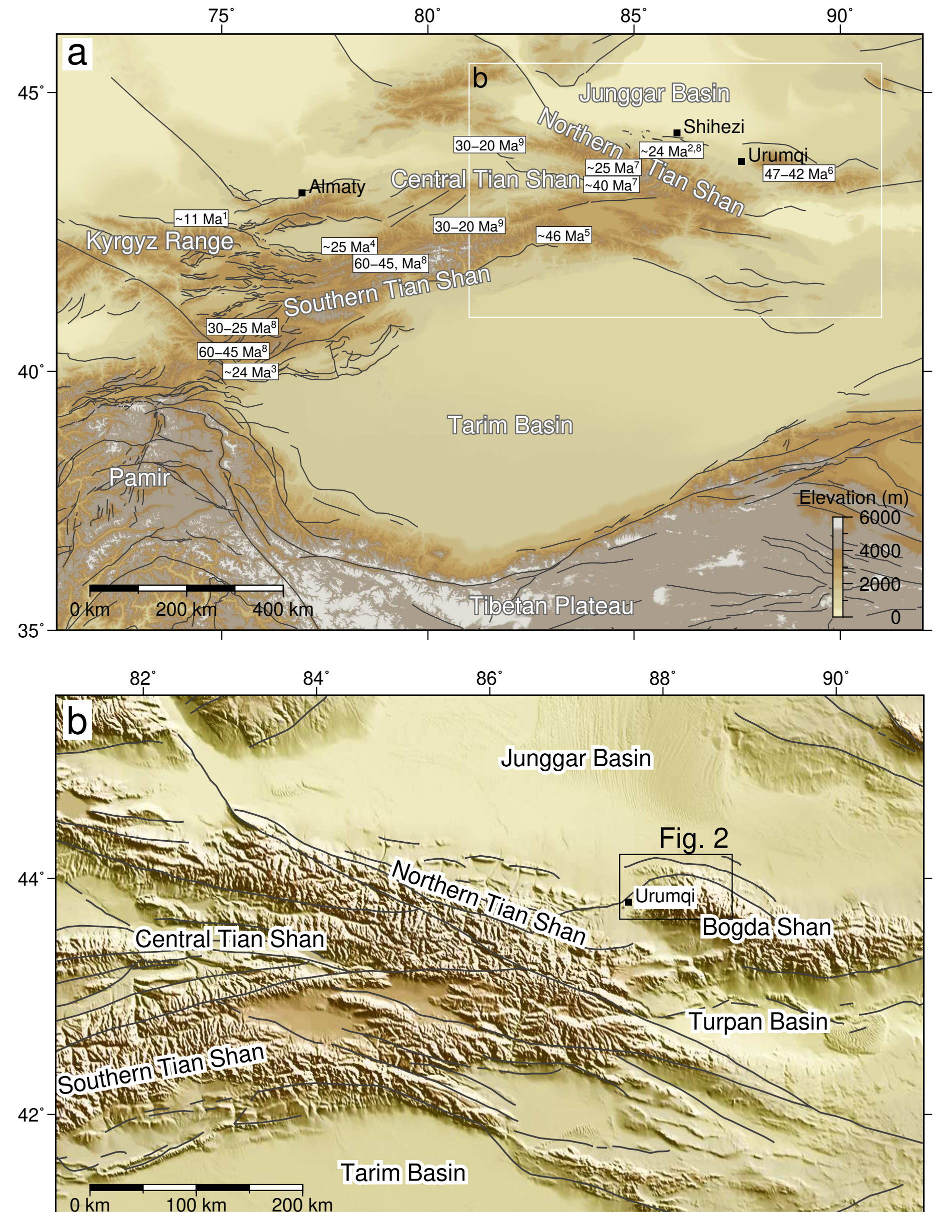

Figure 1: (a) Topography of the Tian Shan and adjacent areas. Age numbers show some representative estimates of the onsets of Cenozoic cooling in different parts of the Tian Shan from thermochronology. Superscripts indicate the references: 1, Bullen et al. (2001); 2, Hendrix et al. (1994); 3, Sobel et al. (2006); 4, Macaulay et al. (2014); 5, Yu et al. (2014); 6, Wang et al. (2008b); 7, Dumitru et al. (2001); 8, Glorie et al. (2011); 9, Wang et al. (2018b). Gray lines depict major active structures in Central Asia (https://esdynamics.geo.uni-tuebingen.de/faults/; Mohadjer et al., 2016). White box indicates the map area of b. (b) Shaded relief map showing the geographic units of the Chinese Tian Shan. Gray lines depict the active structures according to Deng et al. (2003). Box indicates the location of Figure 2.

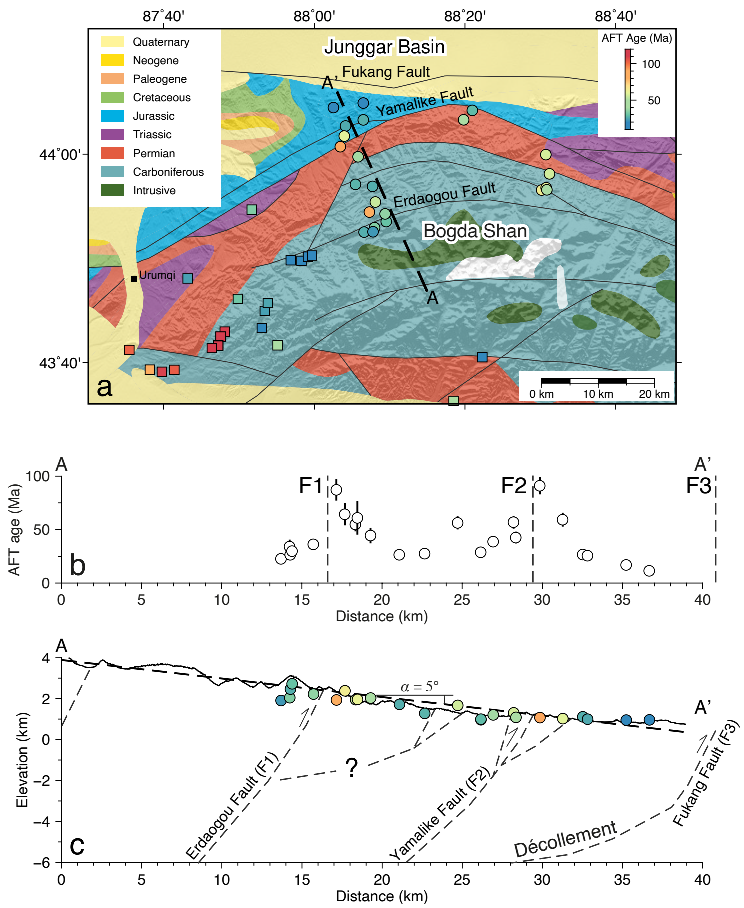

Figure 2: (a) Simplified geological map of the study area (Ye et al., 2017). Colored dots and squares indicate published apatite fission-track (AFT) ages in the area (Zhu et al., 2006; Wang et al., 2007; Shen et al., 2008; Wang et al., 2008b); dots depict ages used to constrain the inverse model and squares not. (b) AFT ages projected to the transect A–A'. Dashed lines indicate surface locations of the major thrust faults. (c) A schematic structural transect on the northern flank perpendicular to the mountain strike, based on which the kinematic model is constructed. Dashed lines depict main structures inferred from the surface structures and nearby geophysical profiles (Wang et al., 2007; Sun and Wang, 2014; Li et al., 2016). Note that the dip of the thrust faults and depth and angle of the décollement are unknown parameters that will be constrained by inverse modeling.

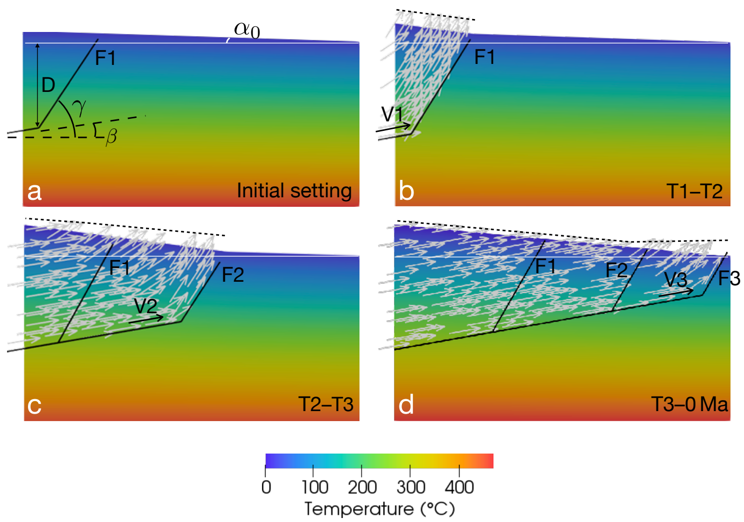

Figure 3: The kinematic model of tectonic evolution for the Bogda Shan. (a) The initial setting with a gently tilted topography. (b–d) Three stages of uplift. We assume that only one fault is active during each stage and forward sequential growth thrust faults in the taper, which is consistent with the prediction of the critical Coulomb wedge theory (Davis et al., 1983; Dahlen et al., 1984; Yuan et al., 2015). Dashed line indicates the uplifted surface of the hanging wall block from the previous model stage assuming that no erosion took place, i.e, the difference between this hypothetical surface and the model surface represents the eroded material. Note that the magnitude of erosion is dependent on the velocity of the rock particles and geometry of the faults. See the text for details of the model setup.

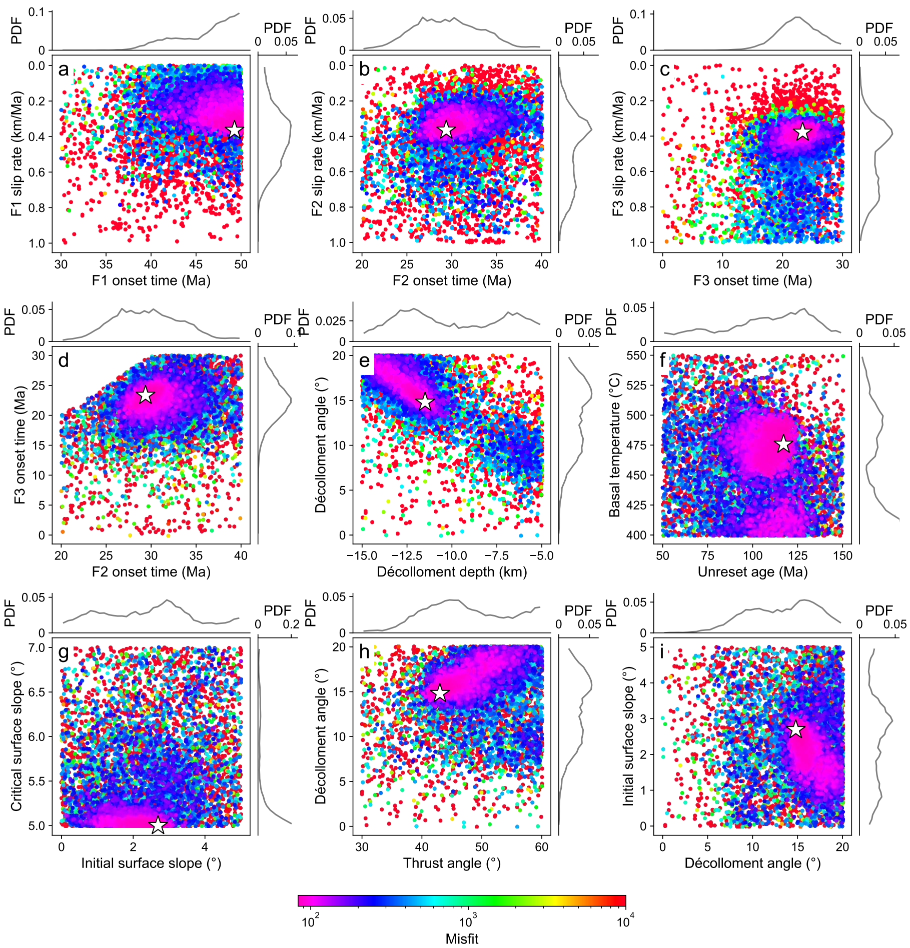

Figure 4: Results of the inverse analysis constrained by AFT age data. Scatter plots show a randomly thinned (10%) ensemble of sampled forward models, projected on planes defined by pairs of parameters. Forward models are color coded according to their misfit values. 1D marginal probability density functions (PDFs) are plotted along the corresponding axes. Stars depict the “best-fit” model.

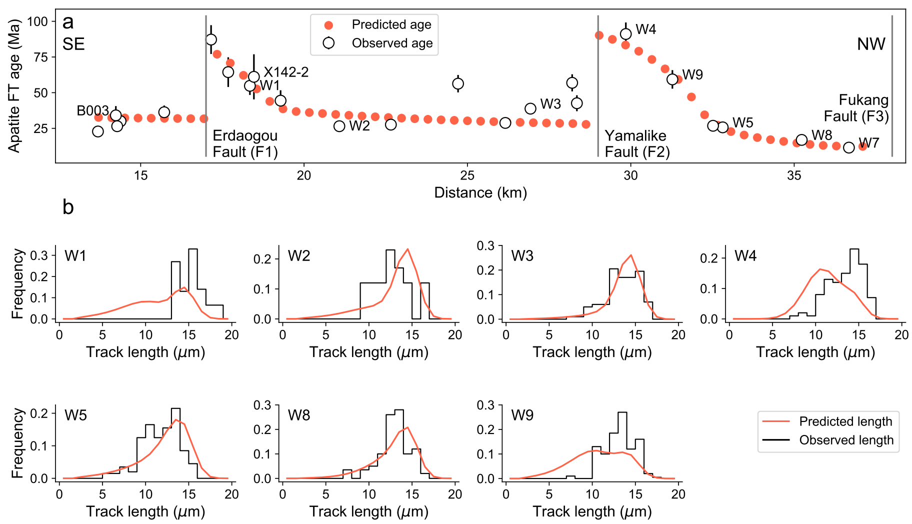

Figure 5: Predicted AFT data by the "best-fit" model compared to the observed data. (a) Predicted and observed AFT ages along the transect across the northern flank of the Bogda Shan. Distances on the transect are the same as the Figure 2b. Vertical lines indicate surface locations of major faults. (b) Predicted (curve) and observed (histogram) AFT length distributions for some samples along the transect. Note that the track length data were not used for inverse modeling.

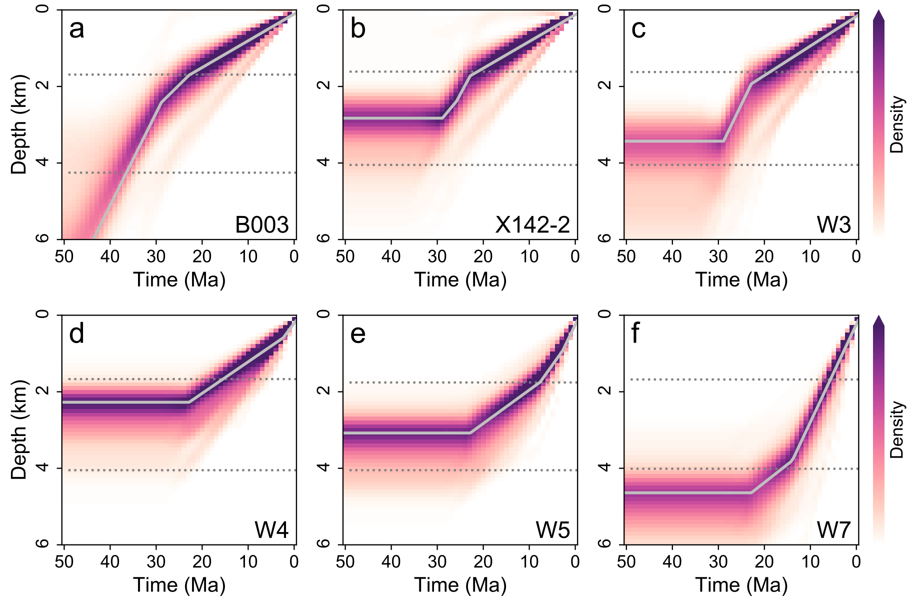

Figure 6: Exhumation histories of representative samples predicted by the inversion. Density plots (color) are calculated from a thinned (10%) ensemble of sampled forward models. Solid lines indicate the "best-fit" models. Dotted horizontal lines indicate boundaries of the partial annealing zone (60–120°C) of apatite fission tracks for the "best-fit" model.

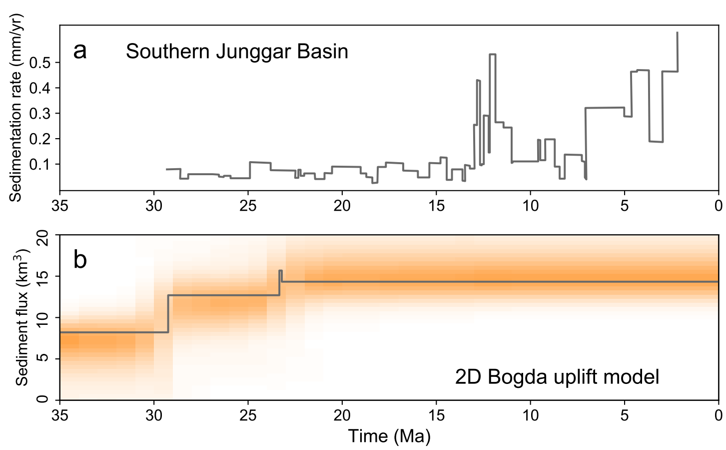

Figure 7: Potential impact of the Cenozoic uplift of the Bogda and northern Tian Shan to sedimentation in the southern Junggar Basin. (a) Sedimentation rate in the southern Junggar Basin inferred from the magnetostratigraphy of a stratigraphic section in the Jingou River (Ji et al., 2008). (b) Sediment flux predicted by the 2D uplift model for a transect across the northern flank of the western Bogda Shan, assuming that the transect has a width of 2 km. Density plot (color) is calculated from a thinned (10%) ensemble of sampled models. Solid line indicate the "best-fit" model.

References

Allen, M.B., Vincent, S.J., 1997. Fault reactivation in the Junggar region, northwest China: The role of basement structures during Mesozoic-Cenozoic compression. Journal of the Geological Society 154, 151–155. doi:10.1144/gsjgs.154.1.0151.

Allen, M.B., Windley, B.F., Chi, Z., Zhong-Yan, Z., Guang-Rei, W., 1991. Basin evolution within and adjacent to the Tien Shan range, NW China. Journal of the Geological Society 148, 369–378. doi:10.1144/gsjgs.148.2.0369.

Avouac, J.P., Tapponnier, P., Bai, M., You, H., Wang, G., 1993. Active thrusting and folding along the northern Tien Shan and Late Cenozoic rotation of the Tarim relative to Dzungaria and Kazakhstan. Journal of Geophysical Research: Solid Earth 98, 6755–6804. doi:10.1029/92JB01963.

Bande, A., Sobel, E.R., Mikolaichuk, A., Schmidt, A., Stockli, D.F., 2017. Exhumation history of the western Kyrgyz Tien Shan: Implications for intramontane basin formation. Tectonics 36, 163–180. doi:10.1002/2016TC004284.

Batt, G.E., Brandon, M.T., Farley, K.A., Roden-Tice, M., 2001. Tectonic synthesis of the Olympic Mountains segment of the Cascadia wedge, using two-dimensional thermal and kinematic modeling of thermochronological ages. Journal of Geophysical Research: Solid Earth 106, 26731–26746. doi:10.1029/2001JB000288.

Bian, S., Gong, J., Chen, L., Zuza, A.V., Chen, H., Lin, X., Cheng, X., Yang, R., 2020. Diachronous uplift in intra-continental orogeny: 2D thermo-mechanical modeling of the India-Asia collision. Tectonophysics 775. doi:10.1016/j.tecto.2019.228310.

Braun, J., 2003. Pecube: A new finite-element code to solve the 3D heat transport equation including the effects of a time-varying, finite amplitude surface topography. Computers and Geosciences 29, 787–794. doi:10.1016/S0098-3004(03)00052-9.

Braun, J., van der Beek, P., Valla, P., Robert, X., Herman, F., Glotzbach, C., Pedersen, V., Perry, C., Simon-Labric, T., Prigent, C., 2012. Quantifying rates of landscape evolution and tectonic processes by thermochronology and numerical modeling of crustal heat transport using PECUBE. Tectonophysics 524-525, 1–28. doi:10.1016/j.tecto.2011.12.035.

Bullen, M.E., Burbank, D.W., Garver, J.I., Abdrakhmatov, K.Y., 2001. Late Cenozoic tectonic evolution of the northwestern Tien Shan: New age estimates for the initiation of mountain building. Bulletin of the Geological Society of America 113, 1544–1559. doi:10.1130/0016-7606(2001)113<1544:LCTEOT>2.0.CO;2.

Caves, J.K., Bayshashov, B.U., Zhamangara, A., Ritch, A.J., Ibarra, D.E., Sjostrom, D.J., Mix, H.T., Winnick, M.J., Chamberlain, C.P., 2017. Late Miocene Uplift of the Tian Shan and Altai and Reorganization of Central Asia Climate. GSA Today doi:10.1130/GSATG305A.1.

Charreau, J., Chen, Y., Gilder, S., Barrier, L., Dominguez, S., Augier, R., Sen, S., Avouac, J.P., Gallaud, A., Graveleau, F., Wang, Q., 2009. Neogene uplift of the Tian Shan Mountains observed in the magnetic record of the Jingou River section (northwest China). Tectonics 28, n/a–n/a. doi:10.1029/2007TC002137.

Coutand, I., Whipp, D.M., Grujic, D., Bernet, M., Fellin, M.G., Bookhagen, B., Landry, K.R., Ghalley, S.K., Duncan, C., 2014. Geometry and kinematics of the Main Himalayan Thrust and Neogene crustal exhumation in the Bhutanese Himalaya derived from inversion of multithermochronologic data. Journal of Geophysical Research: Solid Earth 119, 1446–1481. doi:10.1002/2013JB010891.

Dahlen, F.A., Suppe, J., Davis, D., 1984. Mechanics of Fold-and-Thrust Belts and Accretionary Wedges: Cohesive Coulomb Theory. Journal of Geophysical Research 89, 10087–10101. doi:10.1029/JB089iB12p10087.

Davis, D., Suppe, J., Dahlen, F.A., 1983. Mechanics of fold-and-thrust belts and accretionary wedges. Journal of Geophysical Research 88, 1153. doi:10.1029/JB088iB02p01153.

Deng, Q., Zhang, P., Ran, Y., Yang, X., Min, W., Chu, Q., 2003. Basic characteristics of active tectonics of China. Science in China Series D: Earth Sciences 46, 356–372. doi:10.1360/03YD9032.

Ding, L., Qasim, M., Jadoon, I.A., Khan, M.A., Xu, Q., Cai, F., Wang, H., Baral, U., Yue, Y., 2016. The India–Asia collision in north Pakistan: Insight from the U–Pb detrital zircon provenance of Cenozoic foreland basin. Earth and Planetary Science Letters 455, 49–61. doi:10.1016/j.epsl.2016.09.003.

Dumitru, T.A., Zhou, D., Chang, E.Z., Graham, S.A., Hendrix, M.S., Sobel, E.R., Carroll, A.R., 2001. Uplift, exhumation, and deformation in the Chinese Tian Shan, in: Paleozoic and Mesozoic Tectonic Evolution of Central and Eastern Asia: From Continental Assembly to Intracontinental Deformation, pp. 71–99. doi:10.1130/0-8137-1194-0.71.

England, P., Houseman, G., 1985. Role of lithospheric strength heterogeneities in the tectonics of Tibet and neighbouring regions. Nature 315, 297–301. doi:10.1038/315297a0.

England, P., Molnar, P., 1990. Surface uplift, uplift of rocks, and exhumation of rocks. Geology 18, 1173. doi:10.1130/0091-7613(1990)018<1173:SUUORA>2.3.CO;2.

Gallagher, K., Brown, R., Johnson, C., 1998. Fission Track Analysis and Its Applications To Geological Problems. Annual Review of Earth and Planetary Sciences 26, 519–572. doi:10.1146/annurev.earth.26.1.519.

Gillespie, J., Glorie, S., Jepson, G., Zhang, Z.Y., Xiao, W.J., Danišík, M., Collins, A.S., 2017. Differential Exhumation and Crustal Tilting in the Easternmost Tianshan (Xinjiang, China), Revealed by Low-Temperature Thermochronology. Tectonics 36, 2142–2158. doi:10.1002/2017TC004574.

Gleadow, A.J., Duddy, I.R., 1981. A natural long-term track annealing experiment for apatite. Nuclear Tracks 5, 169–174. doi:10.1016/0191-278X(81)90039-1.

Glorie, S., De Grave, J., Buslov, M.M., Zhimulev, F.I., Stockli, D.F., Batalev, V.Y., Izmer, A., Van den haute, P., Vanhaecke, F., Elburg, M.A., 2011. Tectonic history of the Kyrgyz South Tien Shan (Atbashi-Inylchek) suture zone: The role of inherited structures during deformation-propagation. Tectonics 30, n/a–n/a. doi:10.1029/2011TC002949.

Greene, T.J., Carroll, A.R., Wartes, M., Graham, S.A., Wooden, J.L., 2005. Integrated Provenance Analysis of a Complex Orogenic Terrane: Mesozoic Uplift of the Bogda Shan and Inception of the Turpan-Hami Basin, NW China. Journal of Sedimentary Research 75, 251–267. doi:10.2110/jsr.2005.019.

Gu, Y.f., Ma, M.f., Su, S.l., Xu, H.m., Hu, B., Yao, W.j., 2003. Lithofacies paleogeography of the Cretaceous in the Junggar Basin (in Chinese with English abstract). Petroleum Geology and Experiment 25, 337–342. doi:10.11781/SYSYDZ200304337.

Guo, Z., Zhang, Z., Wu, C., Fang, S., Zhang, R., 2006. The Mesozoic and Cenozoic exhumation history of Tianshan and comparative studies to the Junggar and Altai Mountains (in Chinese with English abstract). Acta Geologica Sinica 80, 1–15.

Heilbronn, G., Boulvais, P., Marchand, E., Robin, C., Bourquin, S., Barrier, L., Jia, Y., Fu, B., Jolivet, M., 2015. Stable isotope characterization of pedogenic and lacustrine carbonates from the Chinese Tian Shan: Constraints on the Mesozoic–Lower Cenozoic palaeoenvironmental evolution. Geochemistry 75, 133–141. doi:10.1016/j.chemer.2014.11.004.

Hendrix, M.S., 1992. Sedimentary record and climatic implications of recurrent deformation in the Tian Shan: evidence from Mesozoic strata of the north Tarim, south Junggar, and Turpan basins, northwest China. Geological Society of America Bulletin 104, 53–79. doi:10.1130/0016-7606(1992)104<0053:SRACIO>2.3.CO;2.

Hendrix, M.S., Dumitru, T.A., Graham, S.A., 1994. Late Oligocene-early Miocene unroofing in the Chinese Tian Shan: an early effect of the India-Asia collision. Geology 22, 487–490. doi:10.1130/0091-7613(1994)022<0487:LOEMUI>2.3.CO;2.

Herbert, T.D., Lawrence, K.T., Tzanova, A., Peterson, L.C., Caballero-Gill, R., Kelly, C.S., 2016. Late Miocene global cooling and the rise of modern ecosystems. Nature Geoscience 9, 843–847. doi:10.1038/ngeo2813.

Herman, F., Copeland, P., Avouac, J.P., Bollinger, L., Maheo, G., Le Fort, P., Rai, S., Foster, D., Pecher, A., Stuwe, K., Henry, P., 2010. Exhumation, crustal deformation, and thermal structure of the Nepal Himalaya derived from the inversion of thermochronological and thermobarometric data and modeling of the topography. Journal of Geophysical Research: Solid Earth 115, B06407. doi:10.1029/2008JB006126.

Herman, F., Cox, S.C., Kamp, P.J., 2009. Low-temperature thermochronology and thermokinematic modeling of deformation, exhumation, and development of topography in the central Southern Alps, New Zealand. Tectonics 28, TC5011. doi:10.1029/2008TC002367.

Hu, X., Garzanti, E., Wang, J., Huang, W., An, W., Webb, A., 2016. The timing of India-Asia collision onset – Facts, theories, controversies. Earth-Science Reviews 160, 264–299. doi:10.1016/j.earscirev.2016.07.014.

Huangfu, P., Li, Z.H., Zhang, K.J., Fan, W., Zhao, J., Shi, Y., 2021. India–Tarim Lithospheric Mantle Collision beneath Western Tibet Controls the Cenozoic Building of Tian Shan. Geophysical Research Letters , e2021GL094561doi:10.1029/2021GL094561.

Hurford, A.J., Green, P.F., 1983. The zeta age calibration of fission-track dating. Isotope Geoscience .

Ji, H., Tao, H., Wang, Q., Qiu, Z., Ma, D., Qiu, J., Liao, P., 2018. Early to Middle Jurassic tectonic evolution of the Bogda Mountains, Northwest China: Evidence from sedimentology and detrital zircon geochronology. Journal of Asian Earth Sciences 153, 57–74. doi:10.1016/j.jseaes.2017.03.018.

Ji, J., Luo, P., White, P., Jiang, H., Gao, L., Ding, Z., 2008. Episodic uplift of the Tianshan Mountains since the late Oligocene constrained by magnetostratigraphy of the Jingou River section, in the southern margin of the Junggar Basin, China. Journal of Geophysical Research 113, B05102. doi:10.1029/2007JB005064.

Jia, Y., Sun, J., Lü, L., 2020. Late Cenozoic tectono-geomorphologic evolution of the northern Tian Shan mountain range: Insight from U-Pb ages of detrital zircon grains from the Upper Oligocene-Quaternary sediments of the southern Junggar basin. Journal of Asian Earth Sciences 194, 104286. doi:10.1016/j.jseaes.2020.104286.

Jolivet, M., Barrier, L., Dauteuil, O., Laborde, A., Li, Q., Reichenbacher, B., Popescu, S.M., Sha, J., Guo, Z., 2018. Late Cretaceous–Palaeogene topography of the Chinese Tian Shan: New insights from geomorphology and sedimentology. Earth and Planetary Science Letters 499, 95–106. doi:10.1016/j.epsl.2018.07.004.

Jolivet, M., Dominguez, S., Charreau, J., Chen, Y., Li, Y., Wang, Q., 2010. Mesozoic and Cenozoic tectonic history of the central Chinese Tian Shan: Reactivated tectonic structures and active deformation. Tectonics 29, TC6019. doi:10.1029/2010TC002712.

Ketcham, R.A., Donelick, R.A., Carlson, W.D., 1999. Variability of apatite fission-track annealing kinetics; III, Extrapolation to geological time scales. American Mineralogist 84, 1235–1255. doi:10.2138/am-1999-0903.

Li, Y., Wang, C., Dai, J., Xu, G., Hou, Y., Li, X., 2015. Propagation of the deformation and growth of the Tibetan–Himalayan orogen: A review. Earth-Science Reviews 143, 36–61. doi:10.1016/j.earscirev.2015.01.001.

Li, Y., Yu, Y., Shen, J., Shao, B., Qi, G., Deng, M., 2016. Active faults and seismogenic models for the Urumqi city, Xinjiang Autonomous Region, China. Earthquake Science 29, 173–184. doi:10.1007/s11589-016-0153-4.

Liu, Y., Wang, Z., Jin, X., Li, T., Li, Y., 2004. Evolution, Chronology and Depositional Effect of Uplifting in the Eastern Sector of the Tianshan Mountains (in Chinese with English abstract). Acta Geologica Sinica 7, 319–331.

Lu, H., Li, B., Wu, D., Zhao, J., Zheng, X., Xiong, J., Li, Y., 2019. Spatiotemporal patterns of the Late Quaternary deformation across the northern Chinese Tian Shan foreland. Earth-Science Reviews 194, 19–37. doi:10.1016/j.earscirev.2019.04.026.

Lü, H.H., Chang, Y., Wang, W., Zhou, Z.Y., 2013. Rapid exhumation of the Tianshan Mountains since the early Miocene: Evidence from combined apatite fission track and (U-Th)/He thermochronology. Science China Earth Sciences 56, 2116–2125. doi:10.1007/s11430-013-4715-1.

Macaulay, E.A., Sobel, E.R., Mikolaichuk, A., Kohn, B., Stuart, F.M., 2014. Cenozoic deformation and exhumation history of the Central Kyrgyz Tien Shan. Tectonics 33, 135–165. doi:10.1002/2013TC003376.

Mohadjer, S., Ehlers, T.A., Bendick, R., Stübner, K., Strube, T., 2016. A Quaternary fault database for central Asia. Natural Hazards and Earth System Sciences 16, 529–542. doi:10.5194/nhess-16-529-2016.

Molnar, P., Tapponnier, P., 1975. Cenozoic Tectonics of Asia: Effects of a Continental Collision: Features of recent continental tectonics in Asia can be interpreted as results of the India-Eurasia collision. Science 189, 419–426. doi:10.1126/science.189.4201.419.

Morin, J., Jolivet, M., Robin, C., Heilbronn, G., Barrier, L., Bourquin, S., Jia, Y., 2018. Jurassic paleogeography of the Tian Shan: An evolution driven by far-field tectonics and climate. doi:10.1016/j.earscirev.2018.10.007.

Najman, Y., Appel, E., Boudagher-Fadel, M., Bown, P., Carter, A., Garzanti, E., Godin, L., Han, J., Liebke, U., Oliver, G., Parrish, R., Vezzoli, G., 2010. Timing of India-Asia collision: Geological, biostratigraphic, and palaeomagnetic constraints. Journal of Geophysical Research: Solid Earth 115. doi:10.1029/2010JB007673.

Pusok, A.E., Stegman, D.R., 2020. The convergence history of India-Eurasia records multiple subduction dynamics processes. Science Advances 6, eaaz8681. doi:10.1126/SCIADV.AAZ8681.

Rak, A.J., McQuarrie, N., Ehlers, T.A., 2017. Kinematics, Exhumation, and Sedimentation of the North Central Andes (Bolivia): An Integrated Thermochronometer and Thermokinematic Modeling Approach. Tectonics 36, 2524–2554. doi:10.1002/2016TC004440.

Rowley, D.B., 1996. Age of initiation of collision between India and Asia: A review of stratigraphic data. Earth and Planetary Science Letters 145, 1–13. doi:10.1016/s0012-821x(96)00201-4.

Sambridge, M., 1999a. Geophysical inversion with a neighbourhood algorithm-I. Searching a parameter space. Geophysical Journal International 138, 479–494. doi:10.1046/j.1365-246X.1999.00876.x.

Sambridge, M., 1999b. Geophysical inversion with a neighbourhood algorithm-II. Appraising the ensemble. Geophysical Journal International 138, 727–746. doi:10.1046/j.1365-246x.1999.00900.x.

Seward, D., Spikings, R., Viola, G., Kounov, A., Ruiz, G., Naeser, N., 2000. Etch times and operator variation for spontaneous track lengths measurements in apatites: an intra-laboratory check. OnTrack 10, 16–21.

Shao, L., Stattegger, K., Li, W., Haupt, B.J., 1999. Depositional style and subsidence history of the Turpan Basin (NW China). Sedimentary Geology 128, 155–169. doi:10.1016/S0037-0738(99)00066-4.

Shen, C., Mei, L., Zhang, S., Liu, L., Tang, J., Zhou, F., Yan, S., Luo, J., 2008. Fission-Track Dating Evidence on Space-Time Difference of Mesozoic-Cenozoic Uplift of the Yilianhabierga Mountain and Bogeda Mountain (in Chinese with English abstract). Journal of Mineralogy and Petrology 28, 63–70.

Shu, L., Wang, B., Zhu, W., Guo, Z., Charvet, J., Zhang, Y., 2011. Timing of initiation of extension in the Tianshan, based on structural, geochemical and geochronological analyses of bimodal volcanism and olistostrome in the Bogda Shan (NW China). International Journal of Earth Sciences 100, 1647–1663. doi:10.1007/s00531-010-0575-5.

Sobel, E.R., Chen, J., Heermance, R.V., 2006. Late Oligocene–Early Miocene initiation of shortening in the Southwestern Chinese Tian Shan: Implications for Neogene shortening rate variations. Earth and Planetary Science Letters 247, 70–81. doi:10.1016/J.EPSL.2006.03.048.

Storti, F., McClay, K., 1995. Influence of syntectonic sedimentation on thrust wedges in analogue models. Geology doi:10.1130/0091-7613(1995)023<0999:IOSSOT>2.3.CO;2.

Sun, Z.m., Wang, Y., 2014. Structural Analysis and Modeling in Miquan Area of the Western Margin of the Bogda Mountain, Xinjiang (in Chinese with English abstract). Geosciences 28, 300–307.

Tagami, T., O'Sullivan, P.B., 2005. Fundamentals of Fission-Track Thermochronology. Reviews in Mineralogy and Geochemistry 58, 19–47. doi:10.2138/rmg.2005.58.2.

Tang, W., Zhang, Z., Li, J., Li, K., Luo, Z., Chen, Y., 2015. Mesozoic and Cenozoic uplift and exhumation of the Bogda Mountain, NW China: Evidence from apatite fission track analysis. Geoscience Frontiers 6, 617–625. doi:10.1016/j.gsf.2014.04.006.

Tapponnier, P., Xu, Z., Roger, F., Meyer, B., Arnaud, N., Wittlinger, G., Yang, J., 2001. Oblique Stepwise Rise and Growth of the Tibet Plateau. Science 294, 1671–1677. doi:10.1126/science.105978.

Van Hinsbergen, D.J., Lippert, P.C., Dupont-Nivet, G., McQuarrie, N., Doubrovine, P.V., Spakman, W., Torsvik, T.H., 2012. Greater India Basin hypothesis and a two-stage Cenozoic collision between India and Asia. Proceedings of the National Academy of Sciences of the United States of America 109, 7659–7664. doi:10.1073/pnas.1117262109.

Wang, C., Dai, J., Zhao, X., Li, Y., Graham, S.A., He, D., Ran, B., Meng, J., 2014. Outward-growth of the Tibetan Plateau during the Cenozoic: A review. Tectonophysics 621, 1–43. doi:10.1016/j.tecto.2014.01.036.

Wang, C., Zhao, X., Liu, Z., Lippert, P.C., Graham, S.A., Coe, R.S., Yi, H., Zhu, L., Liu, S., Li, Y., 2008a. Constraints on the early uplift history of the Tibetan Plateau. Proceedings of the National Academy of Sciences of the United States of America 105, 4987–4992. doi:10.1073/pnas.0703595105.

Wang, J., Cao, Y.C., Wang, X.T., Liu, K.Y., Wang, Z.K., Xu, Q.S., 2018a. Sedimentological constraints on the initial uplift of the West Bogda Mountains in Mid-Permian. Scientific Reports 8. doi:10.1038/s41598-018-19856-3.

Wang, Q., Li, S., Du, Z., 2009. Differential uplift of the Chinese Tianshan since the Cretaceous: Constraints from sedimentary petrography and apatite fission-track dating. International Journal of Earth Sciences 98, 1341–1363. doi:10.1007/s00531-009-0436-2.

Wang, X., Wang, X., Ma, Y., 2007. Differential exhumation history of Bogda Mountain, Xinjiang, Northwestern China since the Late Mesozoic (in Chinese with English abstract). Acta Geologica Sinica 81, 1507–1517.

Wang, Y., Cai, K., Sun, M., Xiao, W., De Grave, J., Wan, B., Bao, Z., 2018b. Tracking the multi-stage exhumation history of the western Chinese Tianshan by apatite fission track (AFT) dating: Implication for the preservation of epithermal deposits in the ancient orogenic belt. Ore Geology Reviews 100, 111–132. doi:10.1016/j.oregeorev.2017.04.011.

Wang, Z., Li, T., Zhang, J., Liu, Y., Ma, Z., 2008b. The uplifting process of the Bogda Mountain during the Cenozoic and its tectonic implication. Science in China, Series D: Earth Sciences 51, 579–593. doi:10.1007/s11430-008-0038-z.

Windley, B.F., Allen, M.B., Zhang, C., Zhao, Z.Y., Wang, G.R., 1990. Paleozoic accretion and Cenozoic redeformation of the Chinese Tien Shan Range, central Asia. Geology 18, 128. doi:10.1130/0091-7613(1990)018<0128:PAACRO>2.3.CO;2.

Wu, C., Wu, G., Shen, J., Dai, X., Chen, J., Song, H., 2016. Late Quaternary tectonic activity and crustal shortening rate of the Bogda mountain area, eastern Tian Shan, China. Journal of Asian Earth Sciences 119, 20–29. doi:10.1016/j.jseaes.2016.01.001.

Wu, J.E., McClay, K.R., 2011. Two-dimensional analog modeling of fold and thrust belts: Dynamic interactions with syncontractional sedimentation and erosion. AAPG Memoir doi:10.1306/13251343M9450.

Xie, W., Luo, Z.Y., Xu, Y.G., Chen, Y.B., Hong, L.B., Ma, L., Ma, Q., 2016. Petrogenesis and geochemistry of the Late Carboniferous rear-arc (or back-arc) pillow basaltic lava in the Bogda Mountains, Chinese North Tianshan. Lithos 244, 30–42. doi:10.1016/j.lithos.2015.11.024.

Yang, S., Li, J., Wang, Q., 2008. The deformation pattern and fault rate in the Tianshan Mountains inferred from GPS observations. Science in China Series D: Earth Sciences 51, 1064–1080. doi:10.1007/s11430-008-0090-8.

Ye, T., Huang, C., Deng, Z., 2017. Spatial database of 1: 2500000 digital geologic map of People's Republic of China. Global Geology Data doi:10.23650/data.H2017.NGA121474.k.1.1.

Yin, A., Nie, S., Craig, P., Harrison, T.M., Ryerson, F.J., Xianglin, Q., Geng, Y., 1998. Late Cenozoic tectonic evolution of the southern Chinese Tian Shan. Tectonics 17, 1–27. doi:10.1029/97TC03140.

Yu, J., Wang, Y., Zheng, D., Zhang, H., Hao, Y., Li, C., Ren, G., Unpublished results. Exhumation of the northern Chinese Tian Shan: Timing and patterns of exhumation deduced from (U-Th)/He thermochronological data .

Yu, S., Chen, W., Evans, N.J., McInnes, B.I., Yin, J., Sun, J., Li, J., Zhang, B., 2014. Cenozoic uplift, exhumation and deformation in the north Kuqa Depression, China as constrained by (U–Th)/He thermochronometry. Tectonophysics 630, 166–182. doi:10.1016/J.TECTO.2014.05.021.

Yuan, X., Maillot, B., Leroy, Y., 2017. Deformation pattern during normal faulting: a sequential limit analysis. Journal of Geophysical Research: Solid Earth 122, 1496–1516.

Yuan, X.P., Leroy, Y.M., Maillot, B., 2015. Tectonic and gravity extensional collapses in overpressured cohesive and frictional wedges. Journal of Geophysical Research: Solid Earth 120, 1833–1854. doi:10.1002/2014JB011612.

Zhang, C.h., Liu, D.b., Zhang, C.l., Wang, Z.q., Yu, Q.x., 2005. Stratigraphic constraints on the initial uplift age of Bogda Shan, Xinjiang, north-west China (in Chinese with English abstract). Earth Science Frontiers , 294–302.

Zhu, W., Shu, L., Wan, J., Sun, Y., Wang, F., Zhao, Z., 2006. Fission-track evidence for the exhumation history of Bogda-Harlik Mountains, Xinjiang since the Cretaceous (in Chinese with English abstract). Acta Geologica Sinica 80, 16–22.